

Flare-induced signals in polarization measurements during the X2.6 flare on 2005 January 15 *

Meng Zhao¹, Jing-Xiu Wang¹, Sarah Matthews², Ming-De Ding³, Hui Zhao¹ and Chun-Lan Jin¹

¹ National Astronomical Observatories, Chinese Academy of Sciences, Beijing 100012, China; zhaomeng@ourstar.bao.ac.cn

² Mullard Space Science Laboratory, University College London, Holmbury St. Mary, Dorking, Surrey, RH5 6NT, UK

³ Department of Astronomy, Nanjing University, Nanjing 210093, China

Received 2008 November 25; accepted 2008 December 29

Abstract Flare-induced signals in polarization measurements which were manifested as apparent polarity reversal in magnetograms have been reported since 1981. We are motivated to further quantify the phenomenon by asking two questions: can we distinguish the flare-induced signals from real magnetic changes during flares, and what we can learn about flare energy release from the flare-induced signals? We select the X2.6 flare that occurred on 2005 January 15, for further study. The flare took place in NOAA active region (AR) 10720 at approximately the central meridian, which makes the interpretation of the vector magnetograms less ambiguous. We have identified that flare-induced signals during this flare appeared in six zones. The zones are located within an average distance of 5 Mm from their weight center to the main magnetic neutral line, have an average size of $(0.6 \pm 0.4) \times 10^{17} \text{ cm}^2$, duration of $13 \pm 4 \text{ min}$, and flux density change of $181 \pm 125 \text{ G}$ in the area of reversed polarity. The following new facts have been revealed by this study: (1) the flare-induced signal is also seen in the transverse magnetograms but with smaller magnitude, e.g., about 50 G; (2) the flare-induced signal mainly manifests itself as apparent polarity reversal, but the signal starts and ends as a weakening of flux density; (3) The flare-induced signals appear in phase with the peaks of hard X-ray emission as observed by the Ramaty High Energy Solar Spectroscopic Imager (RHESSI), and mostly trace the position of RHESSI hard X-ray footpoint sources. (4) in four zones, it takes place contemporarily with real magnetic changes which persist after the flare. Only for the other two zones does the flux density recover to the pre-flare level immediately after the flare. The physical implications of the flare-induced signal are discussed in view of its relevance to the non-thermal electron precipitation and primary energy release in the flare.

Key words: Sun: magnetic field — Sun: flare — Sun: activity

1 INTRODUCTION

Flare-associated changes in the magnetic field are a fundamental issue in solar astrophysics. They are of importance not only in their own right in solar physics, but also in the more general physics of magnetic energy storage and explosive release in phenomena occurring in space and astrophysical plasmas.

* Supported by the National Natural Science Foundation of China.

Taking the observational point of view, but taking no account of the internal physics, flare-associated changes in photospheric magnetic fields largely include two topics: long-term changes before the flare, and short-term changes during the flare. By short-term we mean magnetic changes that occur on the flare time-scale, e.g., from minutes to one or two hours. The former changes are often referred to as the studies of the pre-flare state or the process of flare energy build-up, which cover the temporal range from hours to a few days. This type of study has been reviewed by many authors (Rust 1976; Svestka 1981; Sawyer et al. 1986; Gaizauskas & Svestka 1987; Rust et al. 1994; Sakurai & Hiei 1996; Wang 1998; Wang 2007).

Studies of short-term observed changes during the flare go back to 1981 when Patterson & Zirin (1981) reported “transient magnetic field changes in flares” based on an analysis of Big Bear line-of-sight (LOS) magnetograms and believed that they were real and not instrumental. However, Patterson (1984) later recognized that the reported magnetic transients were not real changes in the magnetic field but could be explained by transient emission of the Fe I 5324 Å line which was used to produce the magnetograms.

Kosovichev & Zharkova (1999) gave a report from an analysis of Michelson Doppler Imager (MDI) magnetograms in which they detected rapid variations of the photospheric magnetic field during an X class flare in AR 8210 on 1998 May 2. They reported that the amplitude of the variations was about 100 G, the characteristic time was 1–5 min, and the spatial scale was 5–20 Mm. Cameron & Sammis (1999) detected a significant change in the longitudinal magnetic fields in NOAA AR 6063 during an X9.3 flare. They used measurements of the LOS field instead of the transverse field to deduce the changes in the horizontal field and avoid a 180° ambiguity. These studies renewed interest in studying rapid magnetic changes on the photosphere during flares.

More recently, Sudol & Harvey (2005) reviewed studies of 20 major flares during the interval 1999 to 2005, aimed at quantifying the longitudinal field changes during flares, and stated that the “abrupt, significant, and permanent changes” of the photospheric longitudinal magnetic field occurred in at least one location within the flaring region during 15 X-class flares. So far, more than 30 major flares have been examined since then and evidence of rapid, significant and persistent changes in both the longitudinal and transverse fields were reported (Wang, Zhao & Zhou 2009). These authors suggest that a flare theory aiming at explaining the full range of solar flare phenomena should confront the new questions raised by the study of magnetic changes during the course of flares.

In the studies of short-term magnetic field changes during flares, many rather confusing terms came forth, viz., transient magnetic field changes in flares (Patterson & Zirin 1981); rapid variations of the photospheric magnetic field (Kosovichev & Zharkova 1999); irreversible changes and more localized and impulsive magnetic field variations (Kosovichev & Zharkova 2001); flare-related magnetic anomalies (Qiu & Gary 2003); apparent sign reversals of magnetic polarities (Qiu & Gary 2003); rapid changes of photospheric magnetic fields (Wang 2007), abrupt, significant, and permanent changes (Sudol & Harvey 2005), rapid, significant and persistent changes (Wang, Zhao & Zhou 2009); and flare induced signals in polarization measurements (Wang, Zhao & Zhou 2009). Different terms reflect different emphases in understanding the short-term observational changes during the flares. ‘Transient magnetic field changes’ and ‘localized and impulsive magnetic field variations’ would imply real physical changes in the photospheric magnetic field during flares, though the reported examples are not necessarily true magnetic changes. Terms such as ‘apparent sign reversal of magnetic polarities’ accurately describe an observational characteristic of flare effects based on polarization measurement; while ‘flare-related magnetic anomaly’ implies abnormal signals in observed magnetograms related to the flare process. The phrase ‘Flare induced signals in polarization measurements’ appears to more clearly indicate the apparent changes in the magnetogram which are not of magnetic origin but induced by flare radiation effects. The other terms refer to the true magnetic changes during the flare in the photosphere based on careful observations (see Sudol & Harvey 2005).

In our first paper of this series (Wang, Zhao & Zhou 2009, Paper I), we drew a distinction between rapid magnetic changes during flares and flare-induced signals in polarization measurements. The former refers to true changes in the magnetic fields; whereas the latter refers to an artifact in polarization measurements as the result of radiative transfer effects in the spectral line formation during a flare, i.e.,

the “flare-related magnetic anomaly” (Qiu & Gary 2003). Throughout the current paper, the terms ‘rapid magnetic changes during flares’ and ‘flare-induced signals’ are used by following the above convention. An example in which the flare-induced signals appeared concurrently with the rapid magnetic changes in the studied flare has been shown in Paper I.

Ding et al. (2002) made a Non-LTE radiative transfer calculation for the spectral line Ni I 6768 Å, which is used by MDI to make magnetic measurements. They found that the line Ni I would appear in emission in the presence of a fairly strong electron beam in a cool atmosphere, and that the profile barely turned to emission if there was no bombarding electron beam, even though the temperature was high. Their result implied that the sign reversal of the longitudinal magnetic field observed in flare events would not be a true reversal but just an artifact associated with the production of an emission profile (Qiu & Gary 2003). The work correctly interprets how non-thermal particle precipitation results in the apparent anomaly in magnetic measurements through non-LTE radiative transfer processes during flares. This provides a vision that the flare induced signal, e.g., the apparent polarity reversal in the LOS magnetograms, contains fundamental information about particle precipitation in flares. Therefore, quantitatively measuring flare-induced polarization signals is not only essential in finding real magnetic changes during the flare, but also an important clue to the flare energy process, e.g., as a further diagnosis for finding where non-thermal particles are bombarding the solar surface.

Unfortunately, so far no detailed quantitative measurements of flare-induced polarization signals have been made. AR 10720 was an active region famous for magnetic complexity and flare prolificacy. It evolved from a β -type sunspot to a large, complex region from 2005 January 10 to 22, and produced 5 X-class flares and 18 M-class flares from January 14 to 21. On January 15, AR 10720 produced an X2.6 flare at 22:25 UT. The flare had its maximum at 23:02 UT and faded away at 23:31 UT. This flare was associated with a halo Coronal Mass Ejection (CME) that left the sun at a speed of 2861 km s^{-1} and a Type II (1151 km s^{-1}) radio sweep. On January 15, the region was fortunately nearest to the solar disk center and we had detailed observations of vector magnetograms from Big Bear Solar Observatory (BBSO) on that day. Therefore, we are able to carry out detailed quantitative measurements on short-term magnetic changes during this major flare, and distinguish between the physical changes of photospheric magnetic fields and particle precipitation signals in the observed magnetograms.

In our first paper of this series, we demonstrated the rapid enhancement of horizontal magnetic fields around the magnetic neutral line in AR 10720 during the X7.1 flare on 2005 January 20 (Wang, Zhao & Zhou 2009). We only briefly mentioned the flare-induced signals in the observed magnetograms, which were localized, impulsive, and spatially correlated with hard X-ray footpoints. The present work aims at examining comprehensive tempo-spatial features of the flare-induced signals in polarization measurements during the X2.6 flare of 2005 January 15. Comparisons between the real magnetic changes in the flare and flare-induced polarization signals are made based on the quantitative analysis. Timing and positioning between flare-induced signals and flare development are also examined.

The next section of the paper is an introduction to our data set and data processing procedures. Section 3 is devoted to descriptions of quantitative results of the observed magnetic changes during the flare. In Section 4, the distinction between the flare-induced signals and rapid magnetic changes during the flare is stressed. In Section 5, we examine the relevance of flare-induced signals to the primary energy release in the flare. Finally, we draw conclusions and discuss the significance of the results presented in this work.

2 DATA SET AND PROCESSING

Vector magnetograms, Ca I 6103 Å images and $H\alpha$ images of AR 10720 were obtained at BBSO in the interval from 16:51 to 23:47 UT which covered the duration of an X2.6 flare well. Soft X-ray data were available from GOES-8 for the observation interval and we also had hard X-ray data from RHESSI (Lin et al. 2002) at the time of the flare’s impulsive phase. Co-alignment between these data sets was achieved using MDI magnetograms (Scherrer et al. 1995) as the intermediary step in some cases. Table 1 summarizes the characteristics of the data used in our analysis.

Table 1 Data Used

Data	Band Center or Energy Level	Cadence (s)	Time Range	Pixel Size (arcsec)	Number
BBSO Magnetogram	6103 Å	80	21:00–23:46	0.61523	187
BBSO Ca I Filtergram	6103 Å	80	22:02–23:47	0.61523	77
BBSO H α Filtergram	0.25 Å	1	21:30–22:54; 23:25–23:59	1.048	120
GOES-8 flux	1–8; 0.5–4 Å	3	21:20–23:50		
RHESSI HX Flux	25–50; 800 keV	4	22:15–23:18		
RHESSI HX image	55–75; 75–95 keV		22:33; 22:49; 23:05	0.0625	5

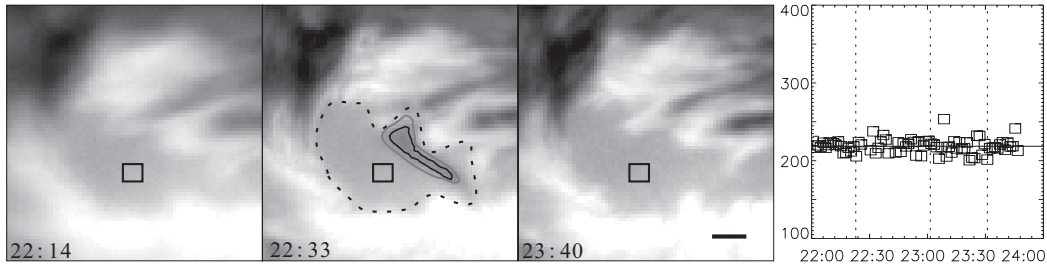


Fig. 1 Panel 1 to Panel 3: three partially enlarged magnetograms around Zone 1. The black solid line indicates the boundary of the area where polarity is reversed. The gray solid line indicates the boundary of the area where the flux density weakened. The dashed line indicates the rough boundary of Zeeman saturation. The box marks the sample region showing the flux variation in the saturated area. Panel 4: variation of the mean magnetic flux density in the sample region from 22:00 to 23:47 UT. The three dashed lines show the start, maximum and end time of the X2.6 flare. The black bar in the lower-right corner denotes a scale of 5 arcsec.

We used data from BBSO's digital vector magnetograph (DVMG, Spirock et al. 2002) system, which covered an area of about $300'' \times 300''$. On 2005 January 15, the camera was configured to be in the 512×512 mode and the pixel resolution was $0.61523''$. The longitudinal magnetic sensitivity was approximately 2 G and the transverse sensitivity was approximately 20 G. The cadence for a complete set of Stokes images was about 80 s. Each data set of BBSO's DVMG consisted of four images: 6103 Å filtergram (Stokes I), LOS magnetogram (Stokes V), and the transverse magnetograms (Stokes U and Q). To avoid anthropogenic influence in flare-induced signal measurement, we did not correct the seeing effect, but rather we just chose the range of data with better seeing. Totally 187 sets of LOS magnetograms from 21:00 to 23:46 UT and 77 pieces of Ca I 6103 Å filtergrams from 22:02 to 23:47 UT were chosen. All the magnetograms were aligned to the same place and bad images were eliminated. The filtergrams of Ca I 6103 Å had the same 80 second time cadence as the LOS magnetograms. The purpose of using the Stokes I filtergrams in this work was to examine the areas of flare induced polarity reversal. If signals appear in both LOS magnetograms and Stokes I filtergrams, it more strongly supports the scenario that the emission profile caused the abnormal signals in the observed magnetograms.

It should be mentioned that the magnetic fields in the AR were so strong that in some sunspot areas there appeared severe saturation in the polarization measurements. Some 'holes' with very low flux density were found in some sunspot umbrae and penumbrae. The saturation is physical in origin. The very strong magnetic fields may render the weak-field assumption invalid in data interpretation. The stray-lights in sunspots may seriously weaken the measured flux density and the large Zeeman separation may require a non-linear calibration. For a filter-based magnetograph, there are not enough measurements available for a physics-based correction of the saturation effects, particularly when only a single spectral line is used in the measurements.

We have developed a geometric method to correct the saturation in the LOS field. Since this is a factitious correction, the extrapolated magnetic field is sensitively influenced by the boundary condition. The resultant error range is even bigger than the flare-induced signals that we were measuring. Fortunately, as shown in Figure 1, the magnetic flux density in the areas of Zeeman saturation did not change much before and during the flare (see the right panel in the figure), so we decided to just leave them uncorrected. In the general case, the saturation would weaken the measured flare-induced signal. Caution needs to be taken when considering the magnitude of flare-induced signals that we have measured in seriously saturated areas.

In Figure 1, the most typical and largest saturation area before the flare, during the flare and after the flare, is shown in a time sequence of subset magnetograms. In the second panel of the figure, the dotted line outlines the boundary of the Zeeman saturation area. The black solid line indicates the area of apparent polarity reversal in the magnetogram, while the grey solid line indicates the area of reducing flux density. To measure the exact area of reducing flux density, we created a relative base difference (RBD) map of the magnetograms by using $M_{\text{rbd}} = (M_i - M_0)/M_0$, where i denoted the magnetogram at time (i). In these maps, all the tiny changes could be seen, and the boundary of the reduced flux density area was determined from these RBD magnetograms. We measured mean magnetic flux density evolution in the box of Figure 1. The magnetic flux density of the saturated area did not change much in the course of the flare so its influence was approximately invariant.

BBSO $H\alpha$ observations had a gap after 22:54 UT. We had a total of 120 $H\alpha$ images from 21:30 UT to 22:54 UT and 23:25 UT to 23:59 UT which were co-aligned by local cross-correlation. The $H\alpha$ filtergrams adopted in this study had a very good consistency in sensitivity and needed no correction. The $H\alpha$ filtergrams helped provide accurate timing of the flare-induced polarization signals throughout the flare, and in particular allowed us to temporally identify the flare-induced signals during the impulsive phase of the flare. Since $H\alpha$ filtergrams were full-disc observations, we produced sub-images of the area of AR 10720. The $H\alpha$ filtergrams and BBSO magnetograms were co-aligned by correlating with the full disk MDI magnetograms.

RHESSI 55–75 and 75–95 keV hard X-ray images are shown at 22:33, 22:49 and 23:05 UT, respectively, to indicate the sites of the particle precipitation during the flare. We saw little evolution in the hard X-ray sources throughout the duration of the flare. We also co-aligned the BBSO magnetograms and RHESSI hard X-ray image through MDI magnetograms by the IDL Map procedures.

3 CHARACTERISTICS OF FLARE-INDUCED SIGNALS IN POLARIZATION MEASUREMENTS

3.1 General Perspectives

Our study began with the detection of observed transient changes in BBSO magnetograms. In all the 187 sets of sequential magnetograms, we noticed that from 22:19 UT to the end of the observation there appeared six zones of significant magnetic polarity reversal. These are the flare-induced signals in polarization measurements. We number them Zones ‘1’ to ‘6’ in this paper roughly according to the time of their first appearance.

In the first column of Figure 2, we show magnetograms at 22:14, 22:33, 22:49 and 23:05 UT, respectively. The top panel of Col. (1) shows the original magnetic structure before the flare. By 22:33 UT, transient magnetic changes in Zones ‘1’, ‘2’ and ‘3’ had already reached their maximum, somewhat before the maximum as seen in hard X-rays; while at 22:49 UT, at the peak of the impulsive phase, transient changes in Zones ‘4’, ‘5’ and ‘6’ became most obvious. In all of the six zones, there appeared localized magnetic polarity reversal, which could be seen in the magnetograms at 22:33 and 22:49 UT, respectively. The changes can be seen more clearly in Col. (2) in the RBD magnetograms. The top panel in this column presents the RBD map of 22:14–22:12 UT, during which no significant zonal transient signal could be seen in the whole AR. The second panel in Col. (2) presents RBD maps of 22:33–22:12 UT and the third and the fourth panel, RBD of 22:49–22:12 and 23:05–22:12 UT. In Col. (2), changes appeared to have larger areas than those in Col. (1) because even small signals were more easily detected when

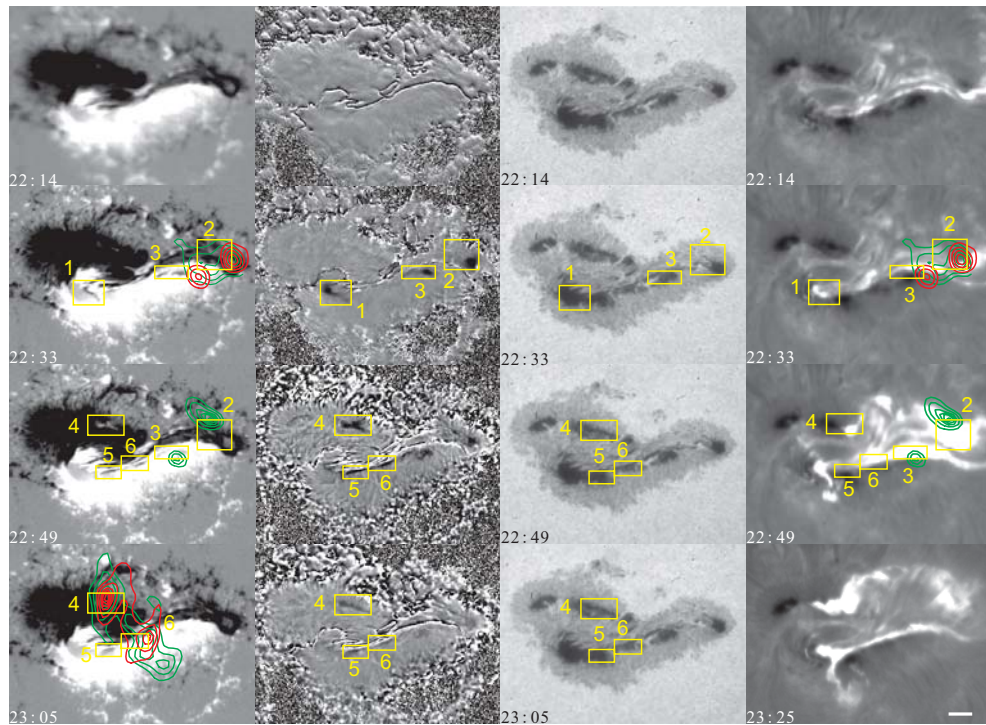


Fig. 2 From Panels 1 to 4 there are LOS magnetograms, RBD magnetograms, Ca I filtergrams and H α filtergrams. Yellow boxes in each column cover the max area of observing changes in all the six zones. They are used to measure magnetic flux. Red and green contours in magnetic field images and H α images are RHESSI hard X-ray sources at 55–75 and 75–95 keV. The white bar in the lower-right corner denotes a scale of 20 arcsec.

relative changes were examined. We adopted the boundary of the transient changes shown in RBD maps to characterize the areas of the flare-induced signals. Yellow boxes in each column cover the maximum areas of each of the zones. They are used to measure apparent flux changes associated with polarity reversal. These apparent flux changes present a measure of how strong the flare-induced signals would be. As soon as the polarity reversal appeared, the total associated flux would clearly drop; and the minimum of the unsigned total flux should correspond exactly to the maximum of the apparent polarity reversal (see Fig. 4).

Col. (3) presents concurrent narrow-band Ca I 6103 Å images. We expect to see enhancement of brightness in the areas of apparent polarity reversal according to the non-LTE calculations made by Ding et al. (2002). However, only faint brightness enhancement could be seen in Zones ‘2’, ‘3’ and ‘6’.

Col. (4) shows BBSO H α images. We use these to measure the H α flare emission in each of the six locations. We also co-aligned the 55–75 and 75–95 keV hard X-ray sources at 22:33, 22:49 and 23:05 UT with the magnetic and H α images. The hard X-ray sources at 22:33 UT and 22:49 UT dovetail well with Zones ‘2’ and ‘3’ in position. These zones represent two large changes in flux density during the polarity reversal. The hard X-ray sources at 23:05 UT dovetail well with Zones ‘4’ and ‘6’ in position. It is noteworthy that Zone 5 shows the largest change in flux density, and a strong temporal correlation with the main peak of the hard X-ray burst and yet, no coincident HXR footpoint source or H α brightening.

Magnetic flux changes related to the polarity reversal in each zone are shown in Figure 3 by blue lines. The gray lines indicate the variation of relative brightness $I_R = \langle I \rangle_i / \langle I \rangle_{AR}$ in the narrow band Ca I images in the six zones, where $\langle I \rangle_i$ and $\langle I \rangle_{AR}$ are the average brightness of zone i and the AR,

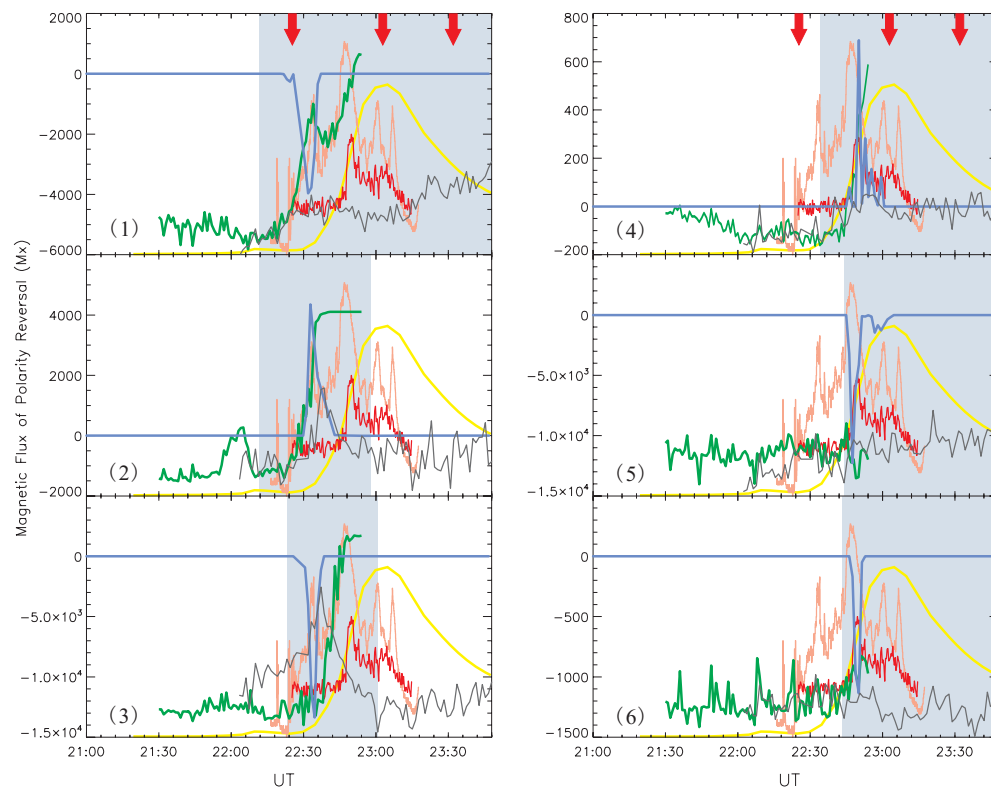


Fig. 3 Curves of magnetic flux changes, Ca I filtergrams brightness changes and H α brightness changes of Zone 1 to Zone 6 in concert with curves of GOES X-ray flux changes and RHESSI hard X-ray flux changes. The blue lines indicate magnetic flux changes of polarity reversal zones. The gray lines indicate variation of relative intensity of Ca I filtergrams. The green lines indicate H α intensity changes. The yellow line is GOES X-ray flux curve and the red line is variation of 800 keV RHESSI hard X-ray flux and the lighter red line is variation of 25–50 keV RHESSI hard X-ray flux. The lighter blue shadow in each panel covers the time range of flux density reduction.

respectively. It can be seen that using the plot of relative brightness makes it easier to see the intensity changes in the photosphere. The curves show relative brightness maxima coinciding with the maximum polarity reversals for Zones ‘1’ to ‘3’, especially for Zones ‘2’ and ‘3’. The green lines indicate H α brightness changes and yellow lines are GOES X-ray flux curves. The red curves show the variation of RHESSI 800 keV hard X-ray flux and the lighter red curves show the variation of RHESSI 25–50 keV hard X-ray flux. The lighter blue shades cover the range of apparent decrease of magnetic flux. The criteria for defining the range are based on whether or not the apparent weakening of the magnetic field could be seen in RBD maps. In principle, the apparent weakening in the magnetic field may result from the flare-induced signals, as well as real changes in magnetic topology and strength.

In this figure, several facts are worth mentioning: (1) all six zones clearly show reversed polarity flux. The reversed signals induced by flare radiation effects for Zones ‘1’, ‘2’, and ‘3’ peak in the flare’s early phase at 22:33 UT in coincidence with an early hard X-ray impulse, for Zones ‘4’, ‘5’, and ‘6’, the induced anomaly peaks in the flare’s impulsive phase at 22:49 UT (see the RHESSI hard X-ray and GOES soft X-ray curves). (2) Most of the zones exhibit an increase in Ca I relative brightness at the photosphere. Among them, the increases in Zones ‘2’ and ‘3’ are most obvious, reaching 5% of the level of the background; while the later polarity reversals in Zones ‘5’ and ‘6’ correspond to the

marginal brightness changes. These observations basically confirm the premise that it is the flare-related emission profile that causes the abnormal polarization signals. (3) $H\alpha$ brightness increases roughly in coincidence with the time range of weakening signals in the magnetograms, especially at the time range of polarity reversal of Zones ‘1’, ‘2’, ‘4’, and ‘6’. For Zone ‘5’, the $H\alpha$ brightness does not show obvious changes. The different behaviors of different zones suggest that the flare-induced signals are caused by very localized effects of flare energy release in polarization measurements.

We note that Zones ‘2’ and ‘3’ show different characteristics compared to the others. First, they have the most significant intensity increase in the photosphere. Secondly, their flux changes recover to the pre-flare level immediately after the flare. In other words, the apparent flux changes are impulsive and really transient in terms of temporal behavior. For the other 4 zones, the flux density does not recover to the pre-flare level, which will be discussed in the following sections. Thirdly, Zones ‘2’ and ‘3’ also happen to be co-spatial with hard X-ray footpoint sources. The scenario of polarity reversal in Zones ‘2’ and ‘3’ is almost completely consistent with Ding et al. (2002) and Qiu & Gary (2003). However, the other zones that show polarity reversals and flux changes seem to need more discussion.

3.2 Quantitative Results

We now discuss a few quantitative perspectives of flare-induced signals in polarization measurements with a summation of our results in a few tables.

3.2.1 Temporal scale

We characterize the temporal scale of the flare-induced signal in two terms: (1) temporal scale of apparent polarity reversal, which is surely the radiative effect of flare emission on the Zeeman measurements; (2) temporal scale of decreasing flux density, which may include both flare effects and real magnetic changes. For each zone, we list in Tables 2 and 3 the start and end time of polarity reversal and flux decrease, and their duration. For polarity reversal, we also list maximum time. The interval of apparent polarity reversal is always covered by the interval of decreasing flux density.

Table 2 Temporal Features of Apparent Polarity Reversal

Zone	Start (UT)	Max (UT)	End (UT)	Duration (min)
1	22:22	22:33	22:36	14
2	22:22	22:32	22:33	11
3	22:31	22:33	22:46	15
4	22:46	22:54	22:59	13
5	22:48	22:49	22:54	6
6	22:46	22:49	23:02	16
Mean				13 ± 4

Table 3 Temporal Features of Decreasing Flux Density

Zone	Start (UT)	End (UT)	Duration (min)
1	22:19	23:47	> 88
2	22:19	22:57	38
3	22:24	22:59	35
4	22:33	23:47	> 74
5	22:46	23:47	> 61
6	22:43	23:47	> 64
Mean			> 60

In summary, the duration of apparent polarity reversal falls in the range of 6–16 min with an average of 13 ± 4 min, which is much longer than the duration of 1–5 min reported by Kosovichev & Zharkova (1999) for an X1 flare on 1998 May 2. The decrease of magnetic flux density started earlier than the polarity reversal. Only for Zones ‘2’ and ‘3’ did the flux density recover to the pre-flare level, and the decrease of magnetic flux density has a duration of 35–38 min. For other zones, the flux changes can be described by a step function during the flare (see Fig. 4) as reported by Sudol & Harvey (2005) for 15 other major flares, and the duration is, at least, longer than one hour. The permanent flux changes suggest that the observed decrease of the magnetic flux dominantly comes from true changes in magnetic topology and field strength in the photosphere during the flare.

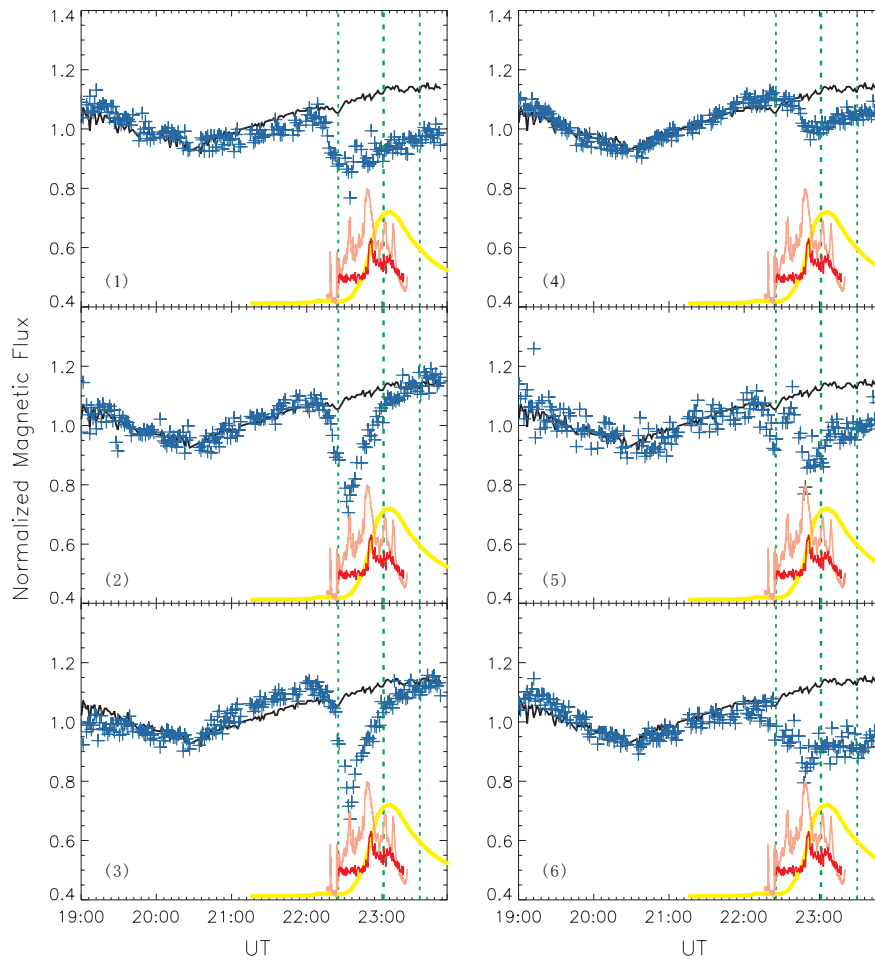


Fig. 4 Relative flux evolution of the whole AR and relative flux evolution of Zone ‘1’ to Zone ‘6’. The black solid lines indicate relative flux evolution of the whole AR and the blue crosses indicate relative flux evolution of Zone ‘1’ to Zone ‘6’. The yellow lines, red lines and light red lines are the same as in Fig. 3. The green vertical dashed lines in each panel indicate the start, maximum and end time of the X2.6 flare.

3.2.2 Spatial scale

Table 4 shows the spatial scales of both decreasing flux density and polarity reversal. The mean area of decreasing flux density of the six zones is $2.9 \pm 1.3 \times 10^{17} \text{ cm}^2$. Zones ‘2’ and ‘3’ present the maximum area of decreasing flux density, which are 6.4 and $10.8 \times 10^{17} \text{ cm}^2$, respectively. Mean area of polarity reversal of the six zones is $0.6 \pm 0.4 \times 10^{17} \text{ cm}^2$, approximately 12 square arcsec. The linear scale is about 3–4 arcsec, i.e., 2–3 Mm. Again, Zones ‘2’ and ‘3’ exhibit the maximum areas of polarity reversal, which are 1.7 and $2.7 \times 10^{17} \text{ cm}^2$, approximately, 30 – 50 square arcsec. If we take the area of polarity reversal as the reliable area of the flare-induced signal, our result is smaller than the early determination of 5–20 Mm (Kosovichev & Zharkova 1999). Similar to the case of temporal scale, the areas of polarity reversal are always embedded within those of decreasing flux density.

Table 4 Spatial Scales of Decreasing Flux Density and Polarity Reversal

Zone	Decreasing Mean	Decreasing Max	Reversal Mean	Reversal Max (10^{17} cm 2)
1	2.8	3.1	0.7	1.0
2	3.2	6.4	0.7	1.7
3	5.2	10.8	1.2	2.7
4	3.2	4.4	0.3	0.5
5	1.8	3.3	0.3	0.5
6	1.4	2.2	0.2	0.4
Mean	2.9 ± 1.3	5.0 ± 3.2	0.6 ± 0.4	1.1 ± 0.9

Table 5 Intensity Features

Zone	Original B_z	Mean Decrease	Mean Reversal	Max Reversal (G)
1	487	227	-96	-232
2	-468	293	188	463
3	739	361	-311	-525
4	-713	227	24	44
5	621	236	-343	-546
6	453	257	-125	-330
Mean	580 ± 128	267 ± 52	181 ± 125	357 ± 195

3.2.3 Magnitude of flux density

We measured the mean flux density before the flare and during the flare in each zone; thus the apparent changes in the magnetograms caused by flare-induced signals could be calculated. The magnetic flux density before the flare, $B_{z_{pre}}$, is the temporal average in the interval from 22:00 to 22:13 UT, before the beginning of the flare. The average flux density during the flare is calculated in the flare interval as shown in Table 3. As listed in Table 5 for these 6 zones, the decrease of average flux density is 267 ± 52 G. The magnetic fields have weakened more than 40%. The maximum decrease of apparent flux in these six zones is more than 700 G.

The apparent polarity reversal took place at magnitudes from several tens to more than 300 G. The temporal average of the reversed field of each zone is -96, 188, -311, 24, -343 and -125 G, respectively, with an absolute mean of 181 ± 125 G. The maximum reversal of flux density in the six zones is over 500 G, and 357 ± 195 G on average.

3.2.4 Timing relative to the flare

The apparent polarity reversal is impulsive and transient in nature. The six zones of polarity reversal can be categorized into two groups according to the timing with respect to the flare. For Zones '1', '2', and '3', polarity reversal took place from 22:22 UT and during the flare's early phase, and coincided with a peak of hard X-ray emission; for the other six zones, it appeared from 23:46 UT and during the flare's impulsive phase, which is characterized by the main peak of hard X-ray emission and rapidly increases in soft X-ray flux and $H\alpha$ brightness. The early flare polarity reversals in Zones '2' and '3', and the later polarity reversal in Zones '4' and '6' are all spatially correlated to hard X-ray foot point sources (see Fig. 2). This clearly indicates that a significant flux of non-thermal high energy electrons is impacting the photosphere in two steps: at the early part of the flare and in the main impulsive phases, respectively, for this X class flare. The apparent polarity reversal in the magnetogram can be used to tempo-spatially trace the high energy particle precipitation.

3.2.5 Positioning with the flare

All the six zones are located within 17 Mm of the magnetic neutral line. The average distance from the weight centers of the polarity reversal to the magnetic neutral line is 5 Mm. The zones with apparent polarity reversal are embedded in sunspot penumbral areas and cover parts of umbral areas of some sunspots.

All zones that have flare-induced signals cover parts of H α flare ribbons (see Figs. 2 and 3). The polarity reversals in Zones ‘2’ and ‘3’, and those in Zones ‘4’ and ‘6’, appear to be in pairs at the positions of hard X-ray footpoint sources with energy ranges of 55–75 and 75–95 keV (see Fig. 2). They took place in the areas of opposite magnetic polarity in the close vicinity of the magnetic neutral line.

3.2.6 Apparent changes in the transverse magnetic fields

So far, the flare-induced signal has only been reported in the circular polarization, which was manifested as an apparent polarity reversal. We have tried to examine whether the zones with polarity reversal also present some measurable changes in the transverse magnetograms. As expected, the noise in the transverse field measurements is much larger, which is reflected by the plots in Figure 5. However, the trend of apparent changes in the transverse fields are rather clear. Note, the transverse field in the observations is good at representing the horizontal field as the AR was at the central meridian.

It is found that all six zones exhibited a clear drop of transverse fields. Similar to the apparent polarity reversal, the drops for Zones ‘2’ and ‘3’ are impulsive and transient. They recovered completely after the flare. Zone ‘2’ exhibited the largest drop in transverse fields, which was approximately 50 G. Zone ‘4’ presented some impulsive changes during the flare’s impulsive phase. Zones ‘1’, ‘5’ and ‘6’ showed permanent weakening of transverse fields from the very beginning of the flare, when compared with the general trend of the transverse field changes of the whole AR. The weakening in these zones is more likely to include the real magnetic changes of horizontal magnetic fields (see Figs. 5 and 6 and description in the next section).

4 CONCURRENT RAPID MAGNETIC CHANGES DURING THE FLARE

To understand the true nature of the apparent flux changes, we compared the relative flux evolution in the polarity reversal zones with the whole AR. Relative flux is defined as $F_r = F_{t(i)}/F_{\text{mean}}$, where $F_{t(i)}$ stands for the flux of the whole AR at time i and F_{mean} is used for the temporal mean magnetic flux of all the observed 187 sets of magnetograms in five hour intervals. In the same way, we defined the relative flux for each zone with polarity reversal. Instead of for the whole AR, in the later case, the F_{mean} would be the temporal mean of the flux for the zone. Relative flux for each zone is also defined in the same way as for the whole AR.

In Figure 4, the black solid lines indicate the relative flux evolution of the whole AR and the blue crosses indicate the relative flux evolution of the six zones. The green vertical dashed lines in each panel are the start, maximum and end times of the X2.6 flare. The yellow line is the GOES X-ray flux curve. The darker red curves and the lighter red curves show the variation of RHESSI hard X-ray flux (800 keV and 25–50 keV). Panel 1 to Panel 6 describe the different trends of flux evolution in the six identified zones, respectively. The flux of Zones ‘1’, ‘4’, ‘5’ and ‘6’ strays away from the main trend of the AR evolution even after the flare, while the flux of Zones ‘2’ and ‘3’ recovers immediately after the flare. Considering whether the apparent changes are recoverable or not – one criterion for distinguishing real magnetic changes from the effects of non-thermal electron bombardment to the solar surface (Sudol & Harvey 2005; Wang, Zhao & Zhou 2009), we believe that in Zones ‘1’, ‘4’, ‘5’ and ‘6’ there exist not only flare-induced signals but also real magnetic changes during the course of the flare.

Since flare-induced signals and real magnetic changes existed together in Zones ‘1’, ‘4’, ‘5’, and ‘6’, we need to reappraise the results we have obtained. In Section 3.2.1, the duration of decreasing flux density in Zones ‘2’ and ‘3’ is actually the duration of the appearance of the flare-induced signal. The same is true for the spatial scales and flux changes in these two zones. They all seem to refer to the

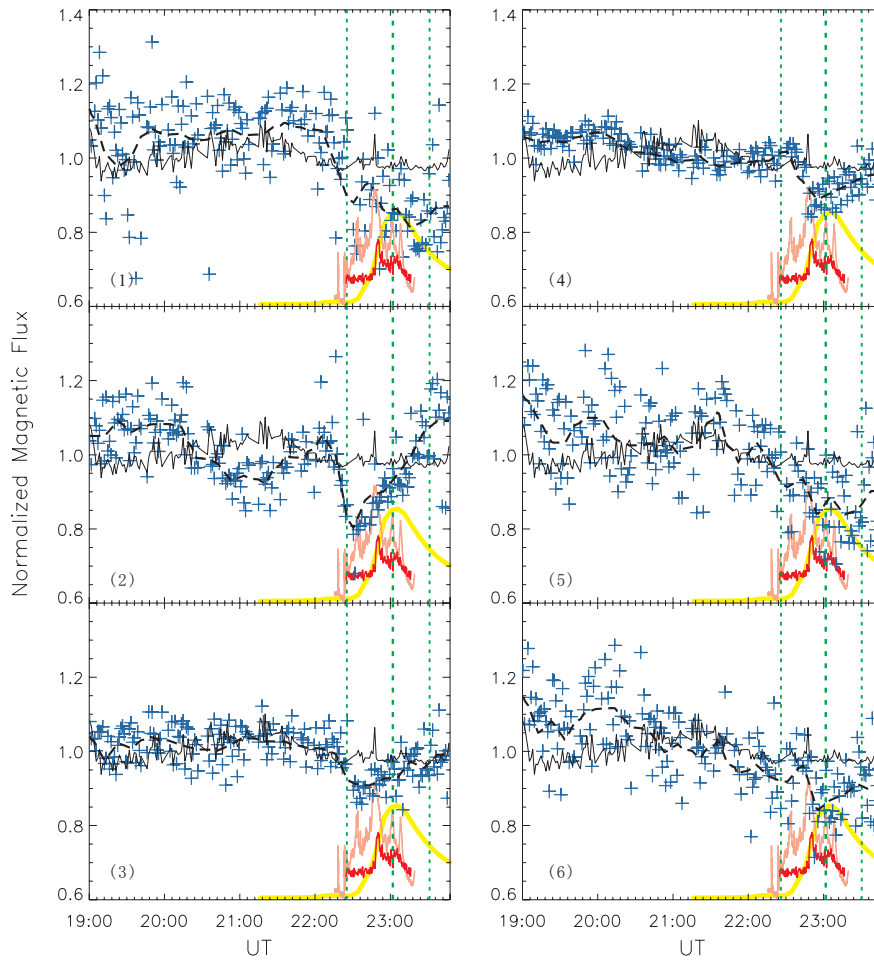


Fig. 5 Relative transverse field evolution of the whole AR and of Zone '1' to Zone '6'. The black solid lines indicate relative transverse field evolution of the whole AR and the blue crosses indicate relative transverse field evolution of Zone '1' to Zone '6'. The dashed lines are 7 min averages of relative transverse field evolution of Zone '1' to Zone '6'. The yellow lines, red lines, lighter red lines and green vertical dashed lines are the same as in Fig. 3.

flare-induced signals. However, the apparent flux changes in Zones '1', '4', '5', and '6' are likely to come predominantly from real magnetic changes, in which flare-induced signals are mixed in a short interval before or at the flare maximum.

For the X7.1 flare on January 20 in the same AR, Wang et al. (2009) detected evidence of horizontal magnetic field changes in the course of the flare. The X7.1 flare appeared close to the west limb (N12W58). The diagnosis had to be made through a geometric analysis and a transform of the vector magnetogram to the heliographic coordinate system. For the current study, the X2.6 flare and the AR were very close to the disk center. It is of great importance to learn whether or not we could detect similar horizontal field changes during this flare.

As shown in Figure 5, although the transverse field measurements show rather large noise compared with the longitudinal field measurements, Zones '1', '4', '5', and '6' show a clear tendency of weakening in the transverse fields when compared with the trend of the horizontal field in the whole AR. These changes are more likely to be real magnetic changes during the flare on the photosphere. We have looked

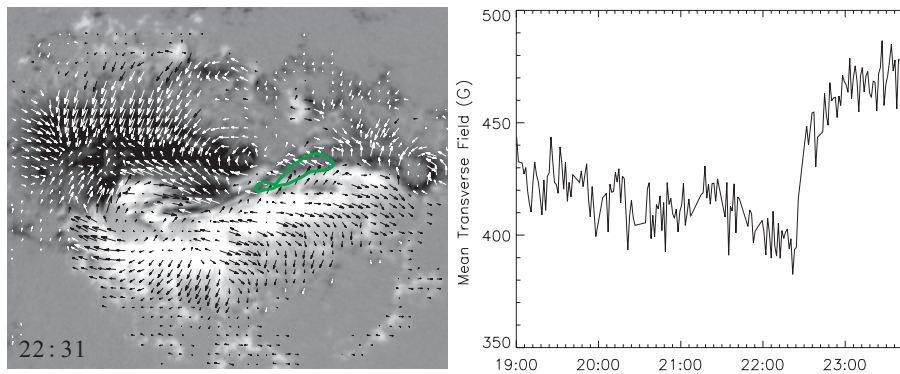


Fig. 6 Left panel: vector magnetograms at 22:31 UT with contour of the area of enhanced horizontal fields. Right panel: changes of the horizontal fields within the contour in the left panel.

for other areas in the AR, particularly in the vicinity of the magnetic neutral line. It is obvious that rapid enhancement of horizontal fields in an extended area centralized on the magnetic neutral line has been found for the X2.6 flare. The area with enhanced horizontal fields is shown by contours in the vector magnetograms in the left panel of Figure 6. The detailed changes of the horizontal fields are shown by the curves in the right panel. This presents another example of rapid, significant, and persistent changes in the horizontal magnetic field in the course of major flares (Wang et al. 2009). As shown in Figure 5, the rather permanent weakening of horizontal fields was found in Zones ‘1’, ‘4’, ‘5’, and ‘6’ during the flare, where the flare-induced polarity reversal appeared in the flare during the flare’s impulsive phase (see Figs. 3 and 4).

Co-existence of the real magnetic changes and the flare-induced signal in the same location is of great interest in learning more about the flare energy release process, and needs more careful discussion.

5 FLARE-INDUCED POLARIZATION SIGNAL AND FLARE ENERGY RELEASE

For a better understanding of the flare-induced signals in the flare, we carry out a non-LTE calculation of the profiles of the Ca I 6103 Å line for the penumbral model atmosphere using a similar method as Ding et al. (2002). We assume that the flaring atmosphere is impacted by a non-thermal electron beam with varying energy fluxes. The calculated Ca I 6103 Å line profiles are shown in the left panel of Figure 7. Similar to the case of the Ni 6768 Å line (Ding et al. 2002), the electron beam bombardment can increase the background continuum opacity and the line source function for the Ca I 6103 Å line, resulting in a line profile with some core emission. Such core emission appears more preferentially in a cool atmosphere like sunspots. However, such an effect is less obvious in the Ca I 6103 Å line than in the Ni 6768 Å line. For the latter, the core emission can exceed the nearby continuum (Ding et al. 2002). For the former, only in the case of strong electron beams can the line profile go from deep absorption to shallow absorption, and then to central-emission that is still below the continuum level. We further construct approximate Stokes V profiles by subtracting the left and right circular polarization components, assumed to have the same shape as the Stokes I profile with a Zeeman splitting induced by a 1 kG magnetic field, which are plotted in the right panel of Figure 7. Such V profiles are not accurate but can serve as qualitative analysis based on their shapes. We find that with the increase of the electron beam flux, the Stokes V profiles would appear from steep to flat slope, and then reverse slope near the core.

The above calculations show us how the non-thermal electron beam can affect the shape of the line profile. We note that a proton beam can play a similar role to an electron beam (see also Zharkova 2008). If no such particle beam is present, the Ca I 6103 Å line changes very little (e.g., Abramenko

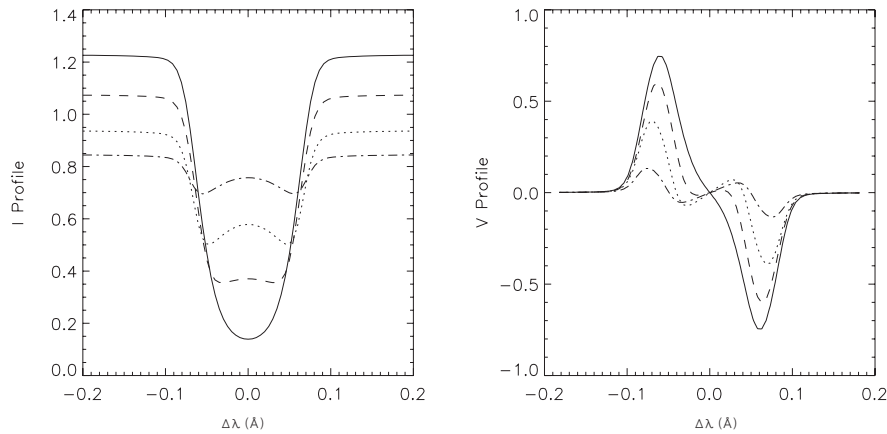


Fig. 7 Left panel: Stokes I profiles of Ca I 6103 Å at the disk center calculated from the sunspot penumbra model, bombarded by an electron beam of energy fluxes: no beam (solid curve), 10^9 (dashed curve), 10^{10} (dotted curve), and 10^{11} $\text{erg cm}^2 \text{s}^{-1}$ (dash-dotted curve). Right panel: deduced Stokes V profiles with an assumed 1 kG total field.

et al. 2004). As in most magnetograph measurements, the calibration for the present data is based on a constant line profile, which does not consider the influence of the change of the profile during the flare. We can therefore draw a picture to explain the flare-induced signal as follows: when the flare occurs in the sunspot area, non-thermal electrons (or protons) can be accelerated in small patches impacting the lower atmosphere; when the electron (proton) beam becomes stronger, and the Ca I 6103 Å line profiles become shallower, leading to a decrease of the magnetic flux density; when the beam is strong enough, central emission appears in the line profile, finally leading to the reversed sign in measurement. In this scenario, evolution from weakening of the flux density to polarity reversal in the magnetograms would indicate a gradual strengthening of electron (proton) beam bombardment. We think that in this flare, the six zones with polarity reversal correspond to the footprints of the high energy particles during flare energy release. As soon as the particle precipitation stops, the magnetic polarity will recover to the original sign.

We should also note that the velocity field, which possibly exists in the chromosphere during the flare, also has an influence on the magnetograph measurements. When the chromosphere is heated, a chromospheric condensation is formed and moves downward, gradually dissipating. Besides, in the sunspot penumbrae, there exist the well-known Evershed flows. These velocity fields make the line profile Doppler shifted, also affecting the magnetograph measurements. Regarding the apparent polarity reversal, in the simulations by Qiu & Gary (2003), only when the velocity field is larger than 10 km s^{-1} can the sign of the magnetic field measured from the Ni I 6768 Å line get reversed. For the setup of the BBSO vector magnetograph, a simple estimation shows that the minimum velocity that will lead to polarity reversal is approximately 4 km s^{-1} upward. However, existence of such a large velocity field in the lower atmosphere lacks sufficient observational evidence for the present event. To our knowledge, a unique study of the flare-associated velocity pattern in flares was made by Harvey & Harvey (1976). They studied eight flare events and found that the maximum increases in velocity ranged from 0.3 to 1 km s^{-1} and were all blue shifted. They also found that the change in velocity began at about 10–15 min prior to the flare's start. The measurements of Evershed flows in sunspots by very high resolution observations of Hinode/SOT revealed a velocity of 1.0 – 1.5 km s^{-1} (Ichimoto et al. 2007). Therefore, we suggest that the velocity field on the photosphere may have an effect in changing the observed magnetic flux, but the relevant Doppler-shift seems unlikely to create the observed sign reversal in usual cases.

Taking the zones of the flare-induced signal as the sites where the non-thermal electrons bombard the photosphere, we are now able to gain information about the primary flare energy release. First,

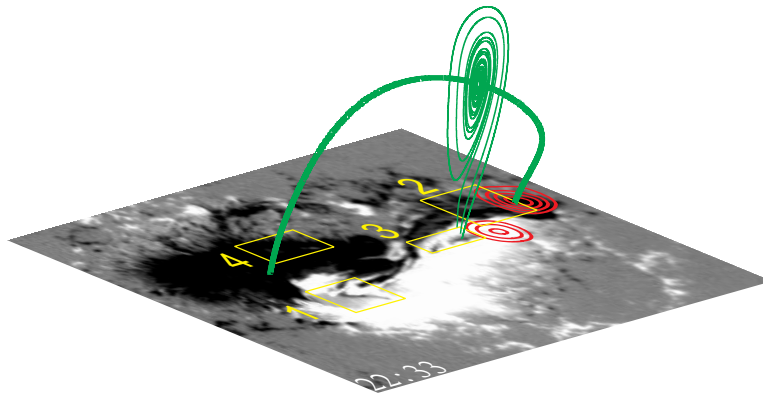


Fig. 8 Topology with a spiral null in the extrapolated magnetic skeleton at 22:19 UT. The green line indicates the fan and spine of the spiral null. The grey-scale map is the magnetogram at 22:33 UT. Red contours indicate RHESSI hard X-ray sources of 55–75 keV.

the high energy particle precipitation takes place in two steps for this X2.6 flare. The first particle precipitation occurs in the flare's early phase at Zones '2' and '3' with its peak coinciding with the first prominent peak of flare HXR emission. The primary energy release is likely to be correlated with this non-thermal electron bombardment. The second step of particle precipitation appears during the flare's impulsive phase, temporally coincident with the main peak of hard X-ray emission. This step of non-thermal electron bombardment is manifested by the flare-induced signals in Zones '4' – '6'. It involves larger areas spreading from the primary energy release site.

Secondly, the high energy particles bombard the photosphere in a long and narrow belt centralized in the region of the magnetic neutral lines, which coincides well with the $H\alpha$ ribbons, unlike most hard X-ray sources. The average distance from the particle precipitation sites to the neutral line is only 5 Mm. The kernel magnetic structures responsible for the primary energy release must have been 'slab-like' in shape, sitting in the magnetic neutral line.

Thirdly, we may take the time-scale and spatial-scale of apparent polarity reversal as that of the particle bombardment. They are approximately 6–16 min and 2–3 Mm, respectively. For this X-class flare, the particle acceleration seems to be longer than for many major flares (eg. the X10 flare on 2003 October 29, Krucker et al. 2005) and is distributed along the whole range of the magnetic neutral line of the AR.

Fourthly, the real magnetic changes and the flare-induced signal appear co-spatially for the second step of particle bombardment. This implies that the magnetic field changes at the peak of the impulsive phase are taking place in the magnetic topology along which the electrons were precipitated into the deep atmosphere at the zones of the later polarity reversal. However, in the first-step particle bombardment, i.e., for the sites of the earlier polarity reversal corresponding to the primary magnetic energy release, the magnetic field involved does not change in topology. However, in the main impulsive phase of the flare, magnetic energy release involves magnetic interaction in structures over the whole AR and results in the structural and field strength changes in accordance with the energy release.

So far, we are not able to construct a very consistent picture of magnetic topology and primary energy release for the X2.6 flare. Zhao et al. (2008) reconstructed the topology skeleton of AR 10720 and studied its gross evolution during this X2.6 flare/CME event. We recognize that the hard X-ray footpoint sources and the primary sites of the flare-induced signal closely correlated with a 3D spiral null revealed by Zhao et al. (2005, 2008). We reconstruct the skeleton of this spiral null at 22:19 UT (see Fig. 8), and find that the spine and fan of this null have their cross-sections at the hard X-ray source and the polarity reversal found in Zones '2' and '3' in the photosphere. According to Zhao et al. (2005, 2008), the spiral null remained during the flare/CME processes, and all other 5 nulls and their skeletons

evolved along with the spiral null and its long spine which lain above the whole range of the magnetic neutral line.

We tentatively suggest that the primary magnetic energy release, e.g., in the form of magnetic reconnection, takes place in association with the spiral null, and the high energy electron beams precipitate into the photosphere along its spine and fan during the primary magnetic reconnection. Later in the flare's impulsive phase, more global magnetic structures are involved in the energy release process with clear topology collapse (see Zhao et al. 2008), and then we see the real magnetic changes during the flare.

6 CONCLUDING REMARKS

By analyzing BBSO vector magnetograms, Ca I 6103 Å and H α images, and related soft and hard X-ray emissions, we have quantified the flare-induced signals during an X2.6 flare of 2005 January 15, and studied the correlation of the flare-induced signal with real magnetic changes during the flare and flare energy release.

It is found that the flare-induced signal, mainly in the form of apparent polarity reversal in the observed magnetograms, takes place in the narrow belt centralized at the magnetic neutral line with an average width of 5 Mm. It has a time scale of 6–16 min, a spatial scale of 2–3 Mm, and a magnitude of reversal flux density of approximate 180 G. A few newly revealed aspects are: (1) The flare-induced signal not only appears in the circular polarization, but also in the transverse magnetograms with slightly less magnitude of about 50 G; (2) The flare-induced signal mainly manifests as apparent polarity reversal, but the signal starts and ends as a weakening of flux density; (3) With regard to the timing, two groups of flare-induced signals are identified – one group happens in the early flare phase, the other in coincidence with the the flare's main impulsive phase. The two groups of flare-induced signals correspond, respectively, with the two-steps of particle bombardment in the flare; (4) The flare-induced signal that appears in the flare's impulsive phase takes place co-spatially with the real magnetic changes which persist after the flare, while for the two zones with the prominent polarity reversal, the flux recovers to the pre-flare level immediately after the flare; (5) For each group of polarity reversal, there is one zone, Zone '1' of the first group and Zone '5' of the second group, for which we could not detect the corresponding hard X-ray source. Moreover, Zone '5' has the deepest reversal in flux density for which we have no clear understanding.

Our observations about the flare-induced signal are generally consistent with the scenario proposed by Ding et al. (2002) and Qiu & Gary (2003). The flare-induced signal in the magnetograms is a radiative transfer effect of the non-thermal electron bombardment on the photosphere in the spectral line formation. A more comprehensive treatment of the non-LTE of Stokes profiles is clearly required for a future study. By following this connection, the flare-induced signal contains fundamental information in monitoring the non-thermal electron bombardment in the explosive flare energy release.

By combining the observations of the flare-induced signal and the real magnetic changes during the flare, we get an opportunity to better understand the flare magnetism and energy processes. It is likely that the first group of flare-induced signals, which occur during the early flare phase, is related to the primary magnetic energy release. It manifests in the form of non-thermal electron acceleration and bombardment without changes in the essential magnetic topology. However, the later group of flare-induced signals during the flare's impulsive phase seem to be related to the main magnetic energy release including more magnetic structure and their rapid changes during the flare. Magnetic eruption or topology collapse must have been involved, like Zhao et al. (2008) proposed. More flare events with more detailed observations are required to establish a consistent physical picture about flare magnetic energy release.

Acknowledgements Many thanks to Professor Haimin Wang and the BBSO staff for providing the excellent data of vector magnetograms and Ca I and H α filtergrams. This work is supported by the National Natural Science Foundation of China (10873020, 10703007, G10573025, 40674081 and 10603008), the CAS Project KJXC2-YW-T04, and the National Basic Research Program of China (G2006CB806303).

References

- Abramenko, V. I., & Baranovsky, E. A. 2004, *Sol. Phys.*, 220, 81
- Cameron, R., & Sammis, I. 1999, *ApJ*, 525, L61
- Ding, M. D., Qiu, J., & Wang, H. 2002, *ApJ*, 576, L83
- Gaizauskas, V., & Švestka, Z. 1987, *Sol. Phys.*, 114, 389
- Harvey, K. L., & Harvey, J. W. 1976, *Sol. Phys.*, 47, 233
- Ichimoto, K., Suematsu, Y., Tsuneta, S., et al. 2007, *Science*, 318, 1597
- Kosovichev, A. G., & Zharkova, V. V. 1999, *Sol. Phys.*, 190, 459
- Kosovichev, A. G., & Zharkova, V. V. 2001, *ApJ*, 550, L105
- Krucker, S., Fivian, M. D., & Lin, R. P. 2005, *Advances in Space Research*, 35, 1707
- Lin, R. P., et al. 2002, *Sol. Phys.*, 210, 3
- Patterson, A., & Zirin, H. 1981, *ApJ*, 243, L99
- Patterson, A. 1984, *ApJ*, 280, 884
- Qiu, J., & Gary, D. E. 2003, *ApJ*, 599, 615
- Rust, D. M. 1976, *Sol. Phys.*, 47, 21
- Rust, D., Kumar, A., et al. 1994, *Sol. Phys.*, 155, 69
- Sakurai, T., & Hiei, E. 1996, *Adv. Space Rev.*, 17, 91
- Sawyer, C., Warwick, J. W., & Dennett, J. T. 1986, *Solar Flare Prediction* (Boulder: Colorado Assoc. Univ. Press)
- Scherrer, P. H., et al. 1995, *Sol. Phys.*, 162, 129
- Spirock, T. J., Yurchyshyn, V. B., & Wang, H. 2002, *ApJ*, 572, 1072
- Sudol, J. J., & Harvey, J. W. 2005, *ApJ*, 635, 647
- Švestka, Z. 1981, *Solar flare Magnetohydrodynamics*, 47
- Wang, H. 2007, *ASP Conf. Series*, 369, 449
- Wang, J. 1998, *ASP Conf. Series*, 140, 121
- Wang, J., Zhao, M., & Zhou, G. 2009, *ApJ*, 690, 862
- Zhao, H., Wang, J. X., Zhang, J., & Xiao, C. J. 2005, *ChJAA (Chin. J. Astron. Astrophys.)*, 5, 443
- Zhao, H., Wang, J., Zhang, J., Xiao, C., & Wang, H. 2008, *ChJAA (Chin. J. Astron. Astrophys.)*, 8, 133
- Zharkova, V. V. 2008, *Sol. Phys.*, 251, 641